Analysis of Ultrasound Propagation in a Metal Rod by Using Finite Element Method

You-xing CHEN(陈友兴)[1,2], Zhao-ba WANG(王召巴)[1,2], Yong JIN(金 永)[2], Ji-liang YANG(杨继亮)[1,2]

(1. *National Key Laboratory for Electronic Measurement Technology, North University of China, Taiyuan* 030051, *China*; 2. *Key Laboratory of Instrumentation Science & Dynamic Measurement (North University of China), Ministry of Education, Taiyuan* 030051, *China*)

Abstract – A metal rod is used in the high temperature testing for ultrasonic propagation and heat output, but the trailing echoes generated by ultrasonic penetration through the metal rod seriously affect the recognition and extraction of characteristic signals. According to the phenomenon, the Finite Element Method (FEM) is used to analyze ultrasonic penetration through a metal rod, the reason of the trailing echoes and the regularity of ultrasonic signals. The motion equation of ultrasonic propagation in a metal rod is established and calculated, then the simulation signals and instantaneous cartographies of the process are obtained. Based on the results of the analysis, it can be concluded that the intervals of the trailing echoes are determined by the rod's diameter and wave velocity. In practical applications, the FEM is used to analyze ultrasonic propagation in the designed buffer rod at first. Based on the characteristics of the simulation signals, the material and dimension are adjusted and selected, aiming to identify the characteristic echo and trailing echoes in time domain and extract characteristic echo from the ultrasonic signals available.

Key words – *ultrasonic propagation*; *FEM*; *finite rod*

Manuscript Number: 1674-8042(2011)04-0312-05

doi: 10.3969/j.issn.1674-8042.2011.04.002

1 Introduction

Ultrasonic testing is effective for measuring thickness, flaws and de-bonds at normal temperatures. Some practical manufacturing processes require on-time testing. It may be performed at rigorous temperatures, e.g. 700 ℃ for aluminum die casting[1], at 200～400 ℃ for polymer extrusion[2,3], and even at temperatures higher than 1 500 ℃ for molten glass and steel[4]. Since a normal temperature is required for the common Ultrasonic Transducer (UT), a metal rod is used as the buffer rod linking up the UT and the tested object in the application[5] for its merits of less attenuation, heat output and more convenience for being fixed. But, due to the impact of the rod's boundary on ultrasonic propagation, the ultrasonic signals present trailing echoes, which seriously affect recognition and extraction of characteristic signals, and even completely submerge the characteristic echo. This has greatly limited the application. In this paper, the process of ultrasonic propagation through a metal rod is emulated by Finite Element Method (FEM).

FEM is an existing technology for analyzing stress wave and ultrasonic propagation[6-9]. The steps of FEM for analyzing ultrasonic propagation are: ① dividing the structure into finite elements; ② analyzing the stress and strain functions of the elements; ③ calculating the structure matrix, including stiffness matrix, inertial matrix and load matrix; ④ establishing and solving the motion equation.

2 Discretization of a metal rod and analysis of the element displacement

Based on the symmetry axiality of the structure of the metal rod, the cylindrical coordinate is used in this paper. z axis is the symmetry axis. All stress, strain and displacement are the function of variables r and z without relation to variable θ. Each node displacement can be expressed as vector addition of the radial displacement u and the axial displacement v. Fig. 1(a) illustrates the discrete triangular mesh of rz cross-section and its numbering method. Any element of the metal rod shown in Fig. 1(b) can be regarded as an annulus formed by a triangular element around the z axis, and any load can also be

* **Received**: 2011-04-30
Project supported: This work was supported by the National Natural Science Foundation of China (No. 60672005), the Shanxi Provincial Foundation for Returned Scholars (Main Program), China (No. 69) and the Science Program of Shanxi Province, China (No. 20110321029).
Corresponding author: You-xing CHEN(chenyouxing@nuc.edu.cn)

viewed as acting on the circle with the nodes. In Fig. 1(a), the numerals are the serial numbers of nodes and the numerals in square brackets are the serial numbers of the elements.

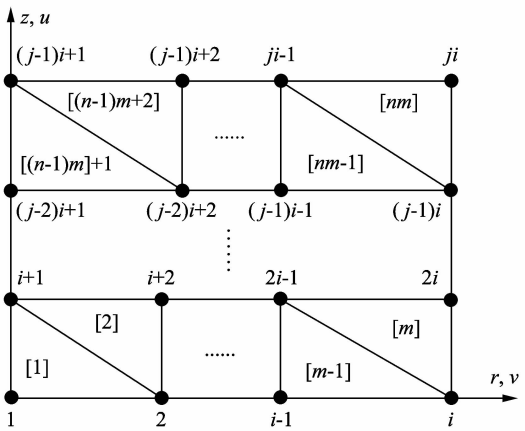

(a) Discretized mesh of *rz* cross-section

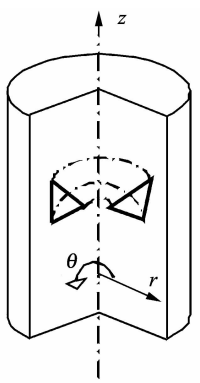

(b) Cyclic element

Fig. 1 Discretized mesh of a metal rod with symmetry axiality

Fig. 2 illustrates a cyclic elements in *rz* cross-section, where i, j, m are the nodes of the element and u, v are the axial displacement and the radial displacement respectively.

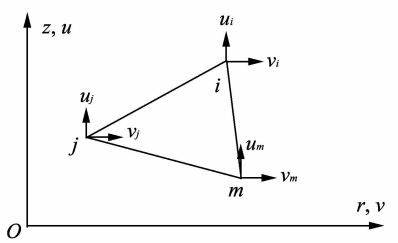

Fig. 2 Three nodes cyclic element in cross-section

So, the node displacement vector of the element is

$$\boldsymbol{a}^e = \begin{bmatrix} \boldsymbol{a}_i \\ \boldsymbol{a}_j \\ \boldsymbol{a}_m \end{bmatrix} = \begin{bmatrix} u_i \\ v_i \\ u_j \\ v_j \\ u_m \\ v_m \end{bmatrix}. \tag{1}$$

Based on the mode of the linear displacement in Ref. [10], Eq. (2) can be obtained as

$$\boldsymbol{u} = \begin{bmatrix} u \\ v \end{bmatrix} = \boldsymbol{N}\boldsymbol{a}^e = \begin{bmatrix} N_i & 0 & N_j & 0 & N_m & 0 \\ 0 & N_i & 0 & N_j & 0 & N_m \end{bmatrix} \begin{bmatrix} u_i \\ v_i \\ u_j \\ v_j \\ u_m \\ v_m \end{bmatrix} \tag{2}$$

where $N_i = \dfrac{a_i + b_i r + c_i z}{2A}$, (i, j, m) are the interpolating functions, $A = \dfrac{1}{2}\begin{vmatrix} 1 & r_i & z_i \\ 1 & r_j & z_j \\ 1 & r_m & z_m \end{vmatrix}$ is the area of the triangle element, $a_i = r_j z_m - r_m z_j$, $b_i = z_j - z_m$, $c_i = r_m - r_j$, and (r_i, z_i) is the coordinate of i node.

The element strain vector is

$$\boldsymbol{\varepsilon} = \begin{bmatrix} \varepsilon_r \\ \varepsilon_z \\ \gamma_{rz} \\ \varepsilon_\theta \end{bmatrix} = \begin{bmatrix} \dfrac{\partial u}{\partial r} \\ \dfrac{\partial v}{\partial z} \\ \dfrac{\partial u}{\partial z} + \dfrac{\partial v}{\partial r} \\ \dfrac{u}{r} \end{bmatrix} = \boldsymbol{B}\boldsymbol{a}^e = [\boldsymbol{B}_i \quad \boldsymbol{B}_j \quad \boldsymbol{B}_m]\boldsymbol{a}^e \tag{3}$$

where $\boldsymbol{B}_i = \dfrac{1}{2A}\begin{bmatrix} b_i & 0 \\ 0 & c_i \\ c_i & b_i \\ f_i & 0 \end{bmatrix}$, $f_i = \dfrac{a_i}{r} + b_i + \dfrac{c_i z}{r}$, (i, j, m)

The element stress vector is

$$\boldsymbol{\sigma} = \begin{bmatrix} \sigma_r \\ \sigma_z \\ \tau_{rz} \\ \sigma_\theta \end{bmatrix} = \boldsymbol{D}\boldsymbol{\varepsilon} = \boldsymbol{D}\boldsymbol{B}\boldsymbol{a}^e = \boldsymbol{S}\boldsymbol{a}^e = [\boldsymbol{S}_i \quad \boldsymbol{S}_j \quad \boldsymbol{S}_m]\boldsymbol{a}^e, \tag{4}$$

where $\boldsymbol{S}_i = \dfrac{E(1-v)}{2A(1+v)(1-2v)}\begin{bmatrix} b_i + A_1 f_i & A_1 c_i \\ A_1(b_i + f_i) & c_i \\ A_2 c_i & A_2 b_i \\ A_1 b_i + f_i & A_1 c_i \end{bmatrix}$,

(i, j, m), $A_1 = \dfrac{v}{1-v}$, $A_2 = \dfrac{1-2v}{2(1-v)}$, E is Young modulus and v is Poisson ration.

On the border of $r = R$, the element stress must require the boundary condition[11]

$$\sigma_r = \sigma_{rz} = 0. \tag{5}$$

3 Composition and calculation of the structure matrix

There are three main structure matrixes. They are structure stiffness matrix $\boldsymbol{K}$, structure inertial matrix $\boldsymbol{M}$ and structure load matrix $\boldsymbol{P}$. They are composed of element stiffness matrix $\boldsymbol{K}^e$, element inertial matrix $\boldsymbol{M}^e$ and node load matrix $\boldsymbol{P}^e$ respec-

tively,

$$\boldsymbol{K} = \sum_e \boldsymbol{K}^e,\ \boldsymbol{M} = \sum_e \boldsymbol{M}^e,\ \boldsymbol{P} = \sum_e \boldsymbol{P}^e. \quad (6)$$

3.1 Element stiffness matrix

The element stiffness matrix of the rod with symmetry axiality is

$$\boldsymbol{K}^e = \int_{V_e} \boldsymbol{B}^{\mathrm{T}}\boldsymbol{D}\boldsymbol{B}\mathrm{d}V = 2\pi\int_{A_e} \boldsymbol{B}^{\mathrm{T}}\boldsymbol{D}\boldsymbol{B}r\mathrm{d}A. \quad (7)$$

Based on the element structure in Fig. 2, Eq. (8) can be obtained as

$$\begin{cases} r \approx \bar{r} = \dfrac{1}{3}(r_i + r_j + r_m), \\ z \approx \bar{z} = \dfrac{1}{3}(z_i + z_j + z_m), \\ f_i = \bar{f}_i = \dfrac{a_i}{\bar{r}} + b_i + \dfrac{c_i\bar{z}}{\bar{r}}, \quad (i,j,m). \end{cases} \quad (8)$$

The explicit expression of element stiffness matrix can be obtained by Eq. (7) and Eq. (8).

$$\boldsymbol{K}^e = 2\pi\bar{r}\boldsymbol{B}^{\mathrm{T}}\boldsymbol{D}\boldsymbol{B}\boldsymbol{A} = \begin{bmatrix} \boldsymbol{K}_{ii} & \boldsymbol{K}_{ij} & \boldsymbol{K}_{im} \\ \boldsymbol{K}_{ji} & \boldsymbol{K}_{jj} & \boldsymbol{K}_{jm} \\ \boldsymbol{K}_{mi} & \boldsymbol{K}_{mj} & \boldsymbol{K}_{mm} \end{bmatrix}, \quad (9)$$

where $\boldsymbol{K}_{rs} = 2\pi\bar{r}\boldsymbol{B}_r^{\mathrm{T}}\boldsymbol{D}\boldsymbol{B}_s A = \dfrac{\pi E(1-\upsilon)\bar{r}}{2A(1+\upsilon)(1-2\upsilon)}\begin{bmatrix} K_1 & K_3 \\ K_2 & K_4 \end{bmatrix}$, $(r,s = i,j,m)$, $K_1 = b_r b_s + f_r f_s + A_1(b_r f_s + f_r b_s) + A_2 c_r c_s$, $K_2 = A_1 c_r(b_s + f_s) + A_2 b_r c_s$, $K_3 = A_1 c_s(b_r + f_r) + A_2 c_r b_s$, $K_4 = c_r c_s + A_2 b_r b_s$.

3.2 Element inertial matrix

The element inertial matrix of the rod with symmetry axiality is

$$\boldsymbol{M}^e = 2\pi\int_{V_e} \rho N^{\mathrm{T}} N\mathrm{d}V = 2\pi\rho\int_{A_e} N^{\mathrm{T}} N r\mathrm{d}A. \quad (10)$$

Based on the relation of the nodes' coordinate in Fig. 2, the explicit expression of the element inertial matrix can be written as

$$\boldsymbol{M}^e = \frac{\pi\rho A}{30}\begin{bmatrix} 6\bar{r}+4r_i & 0 & 6\bar{r}-r_m & 0 & 6\bar{r}-r_j & 0 \\ 0 & 6\bar{r}+4r_i & 0 & 6\bar{r}-r_m & 0 & 6\bar{r}-r_j \\ 6\bar{r}-r_m & 0 & 6\bar{r}+4r_j & 0 & 6\bar{r}-r_i & 0 \\ 0 & 6\bar{r}-r_m & 0 & 6\bar{r}+4r_j & 0 & 6\bar{r}-r_i \\ 6\bar{r}-r_j & 0 & 6\bar{r}-r_i & 0 & 6\bar{r}+4r_m & 0 \\ 0 & 6\bar{r}-r_j & 0 & 6\bar{r}-r_i & 0 & 6\bar{r}+4r_m \end{bmatrix}, \quad (11)$$

where ρ is the density of the metal.

3.3 Element load matrix

The element load matrix of the three nodes is

$$\boldsymbol{P}^e = \begin{bmatrix} \boldsymbol{P}_i \\ \boldsymbol{P}_j \\ \boldsymbol{P}_m \end{bmatrix} = 2\pi\int N^{\mathrm{T}}\begin{bmatrix} T_r \\ T_z \end{bmatrix} r\mathrm{d}A. \quad (12)$$

When the transducer is exciting ultrasonic, side pressure q acts on the front surface of the rod, as shown in Fig. 3. Taking the direction of pressure to boundary as positive, the element surface force can be written as

$$\boldsymbol{T} = \begin{bmatrix} T_r \\ T_z \end{bmatrix} = \begin{bmatrix} 0 \\ q \end{bmatrix}. \quad (13)$$

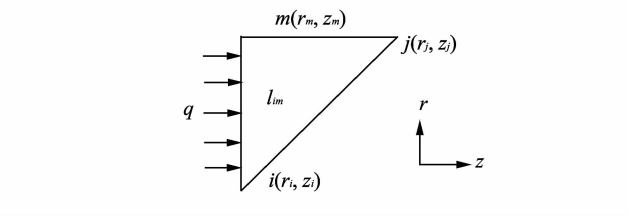

Fig. 3 Side pressure q acting on the element ($z_i = z_m$, $r_m = r_j$)

Taking Eq. (13) into Eq. (12), the node load of the front surface can be obtained as

$$\boldsymbol{p}^e = \begin{bmatrix} \boldsymbol{P}_i \\ \boldsymbol{P}_j \\ \boldsymbol{P}_m \end{bmatrix} = \frac{1}{3}\pi q(r_i - r_m)\begin{bmatrix} 0 \\ (2r_i + r_m) \\ 0 \\ 0 \\ 0 \\ (r_i + 2r_m) \end{bmatrix} \quad (14)$$

Owing to no load acting to the other node, $\boldsymbol{P}^e = 0$.

4 Motion equation of the system

Based on the balance equation, the motion equation can be obtained as

$$\boldsymbol{M}\tilde{\boldsymbol{a}}_t + \boldsymbol{K}\boldsymbol{a}_t = \boldsymbol{P}_t, \quad (15)$$

where $\boldsymbol{a}_t$, $\tilde{\boldsymbol{a}}_t$ and $\boldsymbol{P}_t$ are the node displacement vector, node acceleration vector and structure load matrix respectively in the time of t. Based on the central difference method, the acceleration can be written as

$$\tilde{\boldsymbol{a}}_t = \frac{1}{\Delta t^2}(\boldsymbol{a}_{t-\Delta t} - 2\boldsymbol{a}_t + \boldsymbol{a}_{t+\Delta t}), \quad (16)$$

where Δt is the time step. Taking Eq. (16) into Eq. (15), Eq. (17) can be obtained as

$$\boldsymbol{a}_t = \Delta t^2\boldsymbol{M}^{-1}(\boldsymbol{P}_{t-\Delta t} - \boldsymbol{K}\boldsymbol{a}_{t-\Delta t}) + 2\boldsymbol{a}_{t-\Delta t} - \boldsymbol{a}_{t-2\Delta t}. \quad (17)$$

An aluminum rod with the diameter of 15 mm, length of 100 mm is studied, in which longitudinal and transverse wave velocities are 6 420 m/s and 3 040 m/s, respectively. A transducer with the center frequency of 2.5 MHz and diameter of 14 mm is set on one end of the rod, which sends and receives the ultrasonic wave. In FEM simulation system, the space step is $\Delta l = 0.1$ mm and the time step is $\Delta t = 0.1$ μs, therefore the structure is divided into $150 \times 1\,000 = 150\,000$ circular elements with isosceles right triangle in rz cross-section. Fig. 4(a) is the simulation signals after 5 000 time steps and Fig. 4(b) shows the experiment signals under the same condition of simulation.

From Fig. 4, the simulation signals are in accor-

dance with the experiment signals, and the 1st echo, 2nd echo and higher-order echoes are aroused with equal intervals. Fig. 5 illustrates the instantaneous cartographies of ultrasonic penetration through the rod. Fig. 5(a)~(c) represents the state of the time 4.57 μs, 16.22 μs, 31.75 μs respectively.

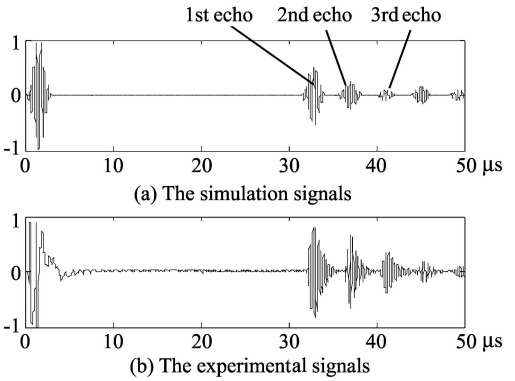

Fig. 4 The simulation signals with FEM

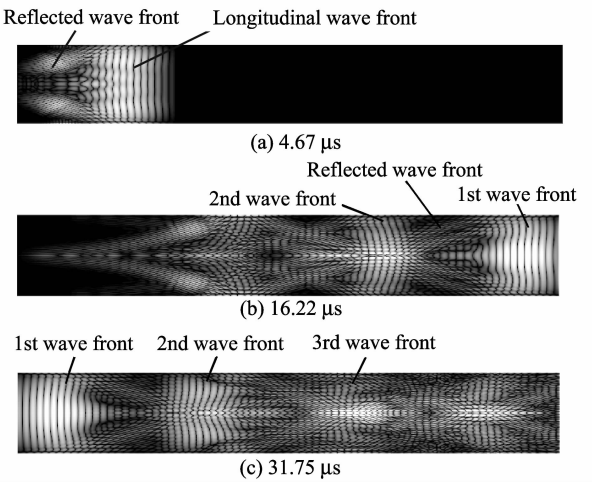

Fig. 5 The instantaneous cartographies of ultrasonic penetration through the aluminum rod

5 Analysis

As shown in Fig. 5, ultrasonic waves propagates along the aluminum rod from the front (left) surface of the rod at the zero time, and the longitudinal wave front and the reflected transverse wave front are aroused as shown in Fig. 5(a). The longitudinal wave front propagates at a speed of the longitudinal wave velocity along the axial. The reflected wave front spreads at a speed of the transverse wave velocity and offsets from the axial with a fixed angle. Mode conversions are occurring as the waves are arriving at the border. Since the propagation direction and velocity of the longitudinal wave are different to those of the transverse wave, the state of Fig. 5(b) is formed as ultrasonic propagation along the aluminum rod. The longitudinal and transverse waves occur alternately, and forms the 1st wave front, the 2nd wave front, and so on, with the transverse wave propagating the interval of the two longitudinal wave fronts. When the 1st wave front arrives at the back (right) surface of the rod, it is reflected by the surface and propagates rightabout. As shown in Fig. 5(c), when the 1st wave front arrives at the left surface again, it is received by the receiver, and forms the 1st echo shown in Fig. 4(a). With the increase of the time, the 2nd wave front, 3rd wave front and so on are all received by the transducer in turn, and form the 2nd echo, 3rd echo, etc. as shown in Fig. 4(a). The 1st wave front propagates at a speed of the longitudinal wave velocity along the axial, so it takes the least time, and the interval of each two close echoes is equal. By using the geometry relationship of sound beam and Snell laws, the interval can be obtained and decided by the rod's diameter, the longitudinal wave velocity and the transverse wave velocity.

$$\Delta T = \frac{D\sqrt{C_l^2 - C_t^2}}{C_l C_t}, \tag{18}$$

where D is the rod's diameter, C_l, C_t are the longitudinal wave velocity and the transverse wave velocity respectively.

6 Conclusions

Owing to the impact of the rod's boundary on ultrasonic propagation in the metal rod, the ultrasonic signals present the trailing echoes after the 1st echo. The trailing echoes seriously affect recognition and extraction of characteristic signal, and even completely submerge it. The ultrasonic propagation in the rod is analyzed by FEM. The conclusion is that the interval of the trailing echoes is decided by the rod's diameter and wave velocity. In practical applications, the FEM is used to analyze ultrasonic propagation in the designed buffer rod. Based on the characteristics of the simulation signals, the material and dimension are adjusted and selected, aiming to identify the characteristic echo and trailing echoes at time domain and extract characteristic echo from the ultrasonic signals available.

References

[1] Z. Sun, C. K. Jen, 2002. Application of ultrasonic in the determination of fundamental wxtrusion performance: monitoring of melt and mixing processes. Polymer Processing Society, 18th annual meeting.

[2] Bo-bing He, Yang Yang, 2005. Fast determination of phase inversion in polymer blends using ultrasonic technique. *Polymer*, (46): 7624-7631.

[3] L. Bourgeois, M. H. Nadal, F. Cl'ement, et. al., 2007. Determination of elastic moduli at high temperatures for uranium vanadium alloy and pure plutonium by an ultra-

sonic method. *Journal of Alloys and Compounds*, (444-445): 261-264.
[4] M. F. Zawrah, M. El-Gazery, 2007. Mechanical properties of SiC ceramics by ultrasonic nondestructive technique and its bioactivity. *Materials Chemistry and Physics*, (106): 330-337.
[5] S. Muthu Kumaran, N. Priyadharsini, V. Rajendran, et. al., 2006. In situ high temperature ultrasonic evaluation for on-line characterization of fine scale precipitation reactions in 8090 Al Li alloy. *Materials Science and Engineering A*, (435-436): 29-39.
[6] D. Data, N. N. Kishore, 1996. Features of ultrasonic wave propagation to identify defects in composite materials modelled by finite element method. *NDT & E International*, 29(4): 213-223.
[7] N. N. Kishore, I. Sridhar, N. G. R. Iyengar, 2000. Finite element modelling of the scattering of ultrasonic waves by isolated flaws. *NDT & E International*, 33: 297-305.
[8] J. J. Wang, Z. H. Shen, X. W. Ni, et. al., 2007. Numerical simulation of laser-generated surface acoustic waves in the transparent coating on a substrate by the finite element method. *Optics & Laser Technology*, 39: 806-813.
[9] Xian-mei Wu, 2000. Studies of rayleigh waves on cylindrical surfaces. The paper for doctor of philosophy, Shanghai: Tongji University.
[10] M. C. Wang, M. Shao, 1997. The fundamentals and numerical method of finite element method. Beijing: Tsinghua University Press, p. 41-43.
[11] Joseph L. Rose, 1999. Ultrasonic waves in solid media. Cambridge Unibersity Press, p. 146-147.